Linear Stability of Coaxial Jets with Application to Aeroacoustics

Dominique C. Perrault-Joncas

Department of Mathematics and Statistics,

McGill University, Montréal

Québec, Canada

February, 2008

A thesis submitted to the Faculty of Graduate Studies and Research

in partial fulfillment of the requirements of the degree of

Master of Science

Your file Votre référence
ISBN: 978-0-494-51321-7
Our file Notre référence
ISBN: 978-0-494-51321-7

Abstract

Motivated by a practical interest in noise generated by turbofan engine, this thesis studies the stability of parallel coaxial jets with velocity and temperature profiles characteristic of the exhaust region of the engine. Because the bypass stream mixes with both the exhaust and the ambient air, these profiles contain thin layers in which the velocity and temperature may vary rapidly. As a consequence, multiple instability modes are possible. In accordance with Rayleigh's theorem for axisymmetric incompressible shear flows, it follows that there are three possible modes, only two of which are unstable. To complement the study of parallel flow stability, this thesis also includes the derivation of the amplitude evolution equation for slowly varying axisymmetric incompressible flows.

Résumé

Cette thèse, motivée par un intérêt pratique pour le bruit généré par les turboventilateurs, étude de la stabilité de jets parallèles ayant des profils de vélocité et de température propres à la région d'échappement. Comme le flux secondaire entre en contact tant avec le gaz d'échappement qu'avec l'air ambiant, ces profils contiennent de minces couches dans lesquelles la vélocité et la température sont portées à varier très rapidement. Par conséquent, de nombreux modes sont possibles. Suivant le théorème de Rayleigh pour les flux incompressibles axisymétriques dans les zones de cisaillement, trois modes sont possibles, dont deux seuls sont instables. En tant que complément de l'étude de la stabilité des flux parallèles, cette thèse inclut également une dérivation de l'équation d'évolution d'amplitude pour les flux incompressibles axisymétriques à variation lente.

Acknowledgments

I wish to thank my thesis supervisor, Professor Sherwin A. Maslowe, for his help, guidance, and support during the crucial phase of this project as well as acknowledge his contribution to the manuscript component of this thesis.

I also wish to acknowledge the *Fonds québécois de la recherche sur la nature et les technologies* for its generous financial support during my years of graduate study in the Master's program at McGill University.

Finally, I would also like to thank Nevena , as well as my parents, Alix and Philippe, for their invaluable support and encouragements.

Table of Contents

List of Figures

Introduction

A good model to predict radiated noise for jet flows is still very much needed today. According to Goldstein [8] direct numerical simulations of the Navier-Stokes equations for compressible flows, is computationally prohibitive. His argument is that the number of mesh points necessary to resolve all the relevant length scales is proportional to the Reynolds number Re, raised to the nine-fourth. For typical jet engine flows, this corresponds to 10^{12} to 10^{15} grid points [8]. This certainly underlines the limits of brute numerical computations. However, it is not the purpose of this thesis to dismiss numerical simulations, which are continuously being improved and obviously contribute to our understanding of the problem. Instead, the aim here is to pursue an alternative, linear stability, to shed light on some of the dynamics at play. In fact, Morris [18], who has been quite involved in the modeling of noise radiation, pointed out "that numerical simulations have made tremendous progress in recent years".

The first model to predict radiated noise, considered as the birth of aeroacoustics as a research area [25], was published in two papers by Lighthill in the early 1950s [11, 12]. The model, known as the acoustic analogy, attempts to identify the origin of noise by rearranging the compressible Navier-Stokes equations into a linear wave equation for the density on the left hand side of the equation and transfer any remaining terms on the left hand side of the equation. The result is a non-homogenous linear wave equation where the non-homogeneous terms are identified as noise sources.

The drawback of this approach is that source terms need to be specified or approximated in some fashion. Indeed, the theory is not self-contained and information about the nature of the turbulence in the flow has to be incorporated before any prediction can be made [25]. Nonetheless, this model proved to be successful at predicting the scaling laws of noise radiation, and a number of improvements were later made to account for such phenomena as the convection and refraction of the waves by the mean flow. In fact, the acoustic analogy model proposed by Lilley [13], which corrected the Lighthill model for the refraction of the waves by the mean flow, is still used today in the most advanced industrial noise prediction methods [8]. Despite its qualities, the acoustic analogy model is unable to account for small changes in the flow, such as the changes produced by noise suppression devices for jet engines. It is precisely this limitation that drives current research in aeroacoustics.

The discovery of large scale turbulence in jet flows in the 1970s by Crow and Champagne [6], led them to propose that these large structures could play an important role in noise generation. Subsequent investigations showed that noise generation has two sources, fine scale turbulence and large turbulence structures [25, 18, 26]. Specifically of interest for this thesis is the large scale turbulence that was found to be an important source of noise for both supersonic and subsonic flows, though to a lesser extent in the case of subsonic flows. The statistical properties of large large turbulence suggests that it can be modeled by mean flow instability waves [25], and many investigations have shown this to be a good model [16]. Most of the stability computations reported to date have been for velocity profiles that involve either discontinuities, i.e. vortex sheets, or else $\bar{u}$ varies slowly with r. We, however, are interested primarily in the stability characteristics of coaxial jets with velocity profiles representative of exhaust conditions for a turbofan engine. In particular, in this thesis we carry out a detailed investigation using velocity and temperature profiles from the coaxial configuration used in the recent experiments of Papamoschou [19].

The link between instability waves and noise generation is not devoid of problems, however. In section 2.2, it is shown that instability waves for axisymmetric jets decay exponentially to zero far away from the jet. This asymptotic behavior, which also holds for two-dimensional jets, implies that there is no acoustic radiation associated with the instability waves themselves, unless the phase speed c_{ph} of the instability wave is equal or greater than the ambient sound speed a_{∞}. Tam and Morris [23] pointed out in 1980 that the problem lay in the parallel flow assumption commonly used for stability analysis. Tam and Burton [24] then showed that this difficulty in the modeling of noise radiated by instabilities could be resolved by taking into account the slow divergence of the jet flow and by extending the resulting solution to the outer field by means of a matched asymptotic expansion [24]. Papers by Benney and Rosenblat, Bouthier, Crighton and Gaster, and Saric and Nayfeh [2, 3, 5, 20] had already been published on the subject of non-parallel effects in jet flows. All these papers employed multiple scales to account for the slow variation of the flow, a method that was first proposed by Benney and Rosenblat [2]. It is Tam and Morris [23], however, that extended this method to the theory of noise radiation.

Interestingly, Bouthier [3] is alone in having considered the propagation of wave packets in slowly diverging jet flows. Even if the primary goal of this thesis is to study the stability characteristics of a parallel coaxial jet, it was deemed worthwhile to investigate how Bouthier's development of the amplitude evolution equation in a two-dimensional jet would apply to axisymmetric jets. The derivation of the amplitude evolution equation for a wave packet is presented in section 1.2.

Returning now to the objectives of the present thesis, we have investigated a number of the factors influencing the stability characteristics of compressible coaxial jets. These include the diameter ratio and the velocity ratio of the primary and secondary streams. In experiments, cold jets are often used for the primary stream, so we have considered both hot and cold jets. The differences between two-dimensional and axisymmetric jets are also of interest and we compare their amplification rates and the number of unstable modes. In the case of coaxial jets, we show that the growth rates are comparable for the $m = 1$ mode and the axisymmetric perturbation, but get smaller for increasing values of m, the azimuthal wavenumber. At subsonic Mach numbers, compressibility does not change the qualitative behavior of unstable modes, except to say that it has a stabilizing effect, so for some comparisons, it is sufficient to study the incompressible case. Before discussing these results in more detail, however, we first present in chapters 1 and 2 the governing equations and the numerical methods that were used to solve them.

Chapter 1

Shear Layer Stability

1.1 Axisymmetric Jet Stability for Parallel Flows

1.1.1 Governing Equations

To obtain the governing equations, we consider small perturbations to a compressible stationary parallel jet with velocity and temperature mean profiles $\bar{\boldsymbol{V}} = (0, 0, \bar{u}(r))$, $\bar{T} = \bar{T}(r)$ in a cylindrical coordinate system (r, θ, x). By combining the continuity, energy and three momentum equations, a single equation can be derived for the radial component of the pressure perturbation $p' = \hat{p}(r)\exp\{i(\alpha x + m\theta - \omega t)\}$. Here the barred variables represent mean profiles, while the primed variables represent small perturbations to the mean profiles. Meanwhile, the hatted variables corresponds to the real eigenfunctions of the perturbations. The link between these variables and the flow variables, $\boldsymbol{V}$, p and ρ , is made explicit in (1.4) below.

We follow Dahl and Morris' [7] derivation and start with the inviscid momentum equations for an ideal gas

$$\rho\,[\frac{\partial \boldsymbol{V}}{\partial t} + (\boldsymbol{V}\cdot\boldsymbol{\nabla})\,\boldsymbol{V}] = -\boldsymbol{\nabla} p, \tag{1.1}$$

the continuity equation

$$\frac{\partial \rho}{\partial t} + \boldsymbol{\nabla} \cdot (\rho \boldsymbol{V}) = 0, \tag{1.2}$$

and the energy equation

$$\frac{\partial p}{\partial t} + (\boldsymbol{V} \cdot \boldsymbol{\nabla})\, p + \gamma\, p(\boldsymbol{\nabla} \cdot \boldsymbol{V}) = 0\ , \tag{1.3}$$

where p is the pressure, $\boldsymbol{V}$ is the velocity, ρ is the density, and γ is the specific heat ratio. Equations (1.1) and (1.2) are the usual momentum and continuity equations, but the derivation of (1.3) deserves some brief comment. For an adiabatic process, the first law of thermodynamics can be written $\rho\, Dh/Dt - Dp/Dt = 0$, where h is the enthalpy. If we assume an ideal gas, then the equation of state is given by $p = \rho\, RT$ and h can be related to the temperature T using c_p, the specific heat at constant pressure. Taking the substantial time derivative of the equation of state, DT/Dt can be replaced by a combination of Dp/Dt and $D\rho/Dt$ and the latter can be eliminated using the continuity equation. We obtain (1.3) finally by noting that $R = c_p - c_v$ and the ratio of specific heats $\gamma = c_p/c_v$, where c_v is the specific heat at constant volume.

The advantage of presenting equations (1.1), (1.2), and (1.3) over starting with linearized equations, as was done by early papers, is that it serves as a convenient starting point for readers who may wish to eventually carry out a nonlinear study. To derive the governing equation for the eigenfunction $\hat{p}(r)$, it is necessary linearize these equations, however. This is done by considering small perturbations of order $\mu \ll 1$ to the mean profiles

$$p = \bar{p} + \mu p', \qquad \boldsymbol{V} = \bar{\boldsymbol{V}} + \mu \boldsymbol{V}', \qquad \rho = \bar{\rho} + \mu \rho'. \tag{1.4}$$

Substituting equations (1.4) into (1.1), (1.2), and (1.3) gives, to $O(1)$, the same equations, i.e. (1.1), (1.2), and (1.3), but for the mean variables $\bar{p}$, $\bar{\boldsymbol{V}}$, and $\bar{\rho}$. Since the profiles are taken to be stationary and parallel in the x-direction, i.e. $\bar{\boldsymbol{V}} = (0, 0, \bar{u}(r))$, $\bar{\rho} = \bar{\rho}(r)$, and since the pressure is constant for a free jet, more specifically

$\bar{p} = 1/(\gamma M_0^2)$, where M_0 is the exhaust Mach number, the μ^0 order equations are automatically satisfied.

To order μ, we obtain the linearized equations for the perturbations p', $\boldsymbol{V}'$, and ρ'

$$\frac{\partial \boldsymbol{V}'}{\partial t} + \bar{\boldsymbol{V}} \cdot \boldsymbol{\nabla} \boldsymbol{V}' + \boldsymbol{V}' \cdot \boldsymbol{\nabla} \bar{\boldsymbol{V}} + \frac{\rho'}{\bar{\rho}} [\bar{\boldsymbol{V}} \cdot \boldsymbol{\nabla} \bar{\boldsymbol{V}}] = -\frac{1}{\bar{\rho}} \boldsymbol{\nabla} p', \tag{1.5}$$

$$\frac{\partial \rho'}{\partial t} + \bar{\boldsymbol{V}} \cdot \boldsymbol{\nabla} \rho' + \boldsymbol{V}' \cdot \boldsymbol{\nabla} \bar{\rho} + \bar{\rho} \boldsymbol{\nabla} \cdot \boldsymbol{V}' + \rho' \boldsymbol{\nabla} \cdot \bar{\boldsymbol{V}} = 0, \tag{1.6}$$

$$\frac{\partial p'}{\partial t} + \bar{\boldsymbol{V}} \cdot \boldsymbol{\nabla} p' + \gamma \bar{p} \boldsymbol{\nabla} \cdot \boldsymbol{V}' + \gamma p' \boldsymbol{\nabla} \cdot \bar{\boldsymbol{V}} = 0. \tag{1.7}$$

Taking the perturbations to be in the form of normal modes, that is $(p', \boldsymbol{V}', \rho') = (\hat{p}(r), \hat{\boldsymbol{V}}(r), \hat{\rho}(r)) \exp\{i(\alpha x + m\theta - \omega t)\}$, where for spatially evolving waves, ω is real and α is complex and the reverse is true for temporally unstable modes, it is straightforward to derive the equation for $\hat{p}$ by substituting into (1.5), (1.6), and (1.7):

$$\frac{d^2 \hat{p}}{dr^2} + \left[\frac{1}{r} - \frac{1}{H} \frac{dH}{dr} \right] \frac{d\hat{p}}{dr} - \left[\alpha^2 \left(1 - M_0^2 H\right) + \frac{m^2}{r^2} \right] \hat{p} = 0\,, \tag{1.8}$$

$$\text{where} \qquad H(r) = \frac{\left(\bar{u} - \omega/\alpha\right)^2}{\bar{T}}. \tag{1.9}$$

To derive (1.8), we made use of the fact that the flow is stationary and parallel in the x-direction once more, and we used the ideal gas law to substitute temperature $\bar{T}(r)$ for the density $\bar{\rho}(r)$. It is important to point out that all variables in (1.8) are dimensionless. Our scaling is identical with that employed in the survey article by Michalke [16], in which velocities are nondimensionalized with respect to the exhaust velocity and temperature at $r = 0$, u_0 and T_0 (so $\bar{u}(0) = 1$ and $\bar{T}(0) = 1$). Consistent with that choice, the pressure and sound speed of the primary stream are used in defining M_0, the exhaust Mach number. The boundary conditions for equation (1.8) require that $\hat{p}$ be bounded as $r \to 0$ and that $\hat{p}$ tend to zero for $r \to \infty$. More will be said about the boundary conditions in section 2.2.

1.1.2 Eigenvalue Problem

Equation (1.8), derived in the previous section, describes an eigenvalue problem for the pressure perturbation $\hat{p}$. When studying spatial instabilities, the eigenvalue is the complex wavenumber $\alpha = \alpha_r + i\alpha_i$, which is obtained for a given real frequency ω and azimuthal wavenumber m. The reverse is true for temporally unstable modes, i.e. the eigenvalue is the complex frequency, obtained for a given real wavenumber. The resulting dispersion relation for spatial instabilities takes the form $\alpha = \alpha(\omega, m)$ for a given wavenumber m. Because the perturbations are in the form of normal modes and are proportional to $\exp\{i(\alpha x + m\theta - \omega t)\}$, they will be spatially unstable if $\alpha_i < 0$, neutral if $\alpha_i = 0$, and damped if $\alpha_i > 0$.

Given that most of our results exhibit qualitative behavior that is similar for both incompressible and compressible jets, let us begin by briefly reviewing the stability theory for the incompressible case. For plane parallel flows, the first important result is Rayleigh's inflection point theorem. This theorem states that a necessary condition for instability is that $\bar{u}''$ change sign at some point in the flow [15]. In other words, $\bar{u}''$ must vanish at some point in the flow and, from a physical point of view, this amounts to saying that the vorticity $\bar{u}'$ must have an extremum. Building on this result, Fjørtoft went on to show that an additional necessary condition for instability is that the absolute value of the vorticity has to be local a maximum at the inflection point.

The generalization of Rayleigh's inflection point theorem to parallel axisymmetric flows is the following (see Batchelor and Gill [1]): a necessary condition for instability is that the quantity $Q'(r) = 0$ for some value of r, where

$$Q(r) = \frac{r\,\bar{u}\,'}{m^2 + \alpha^2 r^2} \quad . \tag{1.10}$$

A further condition derived by Batchelor and Gill is the axisymmetric analogue of Fjørtoft's theorem. It requires that $|\frac{d\bar{u}}{d\rho}|$, be a maximum at the point of inflection with respect to ρ, where ρ is given by (1.12). More will be said about the variable ρ and its relation with Rayleigh's inflection point theorem below. Batchelor and Gill also showed that Howard's semi-circle theorem applies to axisymmetric flows. This means that the only neutral modes that are the limit of unstable modes are those for which $\bar{u} = \omega/\alpha$ at the value of r for which $Q'(r) = 0$.

A particularly significant feature of the stability criterion (1.10) is its dependence on m, the azimuthal wavenumber. This is in contrast to Rayleigh's inflection point theorem for two-dimensional flows which involves only the velocity profile. An illustrative example considered by Batchelor and Gill is the velocity profile

$$\bar{u} = \frac{1}{(1+r^2)^2} \tag{1.11}$$

which, according to (1.10), is stable to axisymmetric $m = 0$ perturbations. These authors also showed, by considering neutral modes and the real part of the semicircle theorem, that as $m \to \infty$ axisymmetric flows are stable and, as a consequence, for the velocity profile (1.11) it turns out that only the non-axisymmetric $m = 1$ mode can be unstable. Growth rates were not computed, but the critical wavenumber below which instability can occur was estimated to be $\alpha = 1.46$.

The obvious question to now address is the following: what is the relationship of the foregoing stability criteria for plane parallel flows to the axisymmetric case? The fact that the two-dimensional results are pertinent was made clear by Batchelor and Gill who pointed out that a change in the radial coordinate to

$$\rho = m^2 \log r + \alpha^2 r^2/2 \tag{1.12}$$

changes the stability criterion (1.10) to be that $\bar{u}(\rho)$ has an inflection point. One difference, however, is that for an axisymmetric jet such as the one illustrated in Fig. 2.1, we would consider only half of the profile, given that $0 \leq r < \infty$. Although this reduces the number of unstable modes, the possibility of non-axisymmetric perturbations can lead to additional instabilities, as already noted above for the velocity profile (1.11).

1.2 Amplitude Evolution Equation for Slowly Varying Axisymmetric Flows

Perturbations rarely consist of single wavelengths, as has been considered so far in subsections 1.1.1 and 1.1.2. In fact, as mentioned at the end of the introduction, such monochromatic instability waves cannot model noise generation. A number of authors have addressed this problem by taking into account the slow divergence of the jet in the x-direction through the use of multiple scales expansions [23, 24, 7]. However, none of these authors considered the propagation of wave packets in slowly diverging jets. The exception to this is Bouthier [3], who looked at a slowly diverging two-dimensional flow, though not in the context of aeroacoustics.

In the interest of seeing how Bouthier's method [3] applies to axisymmetric jet flows and as a starting point for future numerical work on the aeroacoustics of slowly diverging coaxial jets, what follows is a derivation of the amplitude evolution equation for incompressible slowly varying jets for axisymmetric disturbances. The derivation is restricted to incompressible jets and disturbances with no azimuthal dependence in order to keep the algebra more manageable, but the method presented here would still apply if these restrictions were lifted. For ease of reference, we tried to keep the notation as close as possible to Bouthier's. However, to avoid confusion with other variables already used in this thesis or to clarify certain steps, it was deemed necessary to change some of the notation.

The assumption that the flow is incompressible means that the continuity equation (1.2) can be solved by using a stream function ψ. For an axisymmetric flow $\boldsymbol{V} = (v, 0, u)$ using the cylindrical coordinates (r, θ, x), the stream function is given by $\psi_r/r = u$ and $\psi_x/r = -v$. Substituting the stream function into the momentum equations (1.1) and taking the curl gives the vorticity equation

$$\frac{\partial \psi}{\partial r}\frac{\partial^2 \psi}{\partial x \partial r} + \frac{1}{r}\frac{\partial \psi}{\partial x}\frac{\partial \psi}{\partial r} - \frac{\partial \psi}{\partial x}\frac{\partial^2 \psi}{\partial r^2} = 0. \tag{1.13}$$

We then employ the same method as in subsection 1.1.1 to linearize the equation (1.13). Again, we introduce small perturbations of order $\mu \ll 1$ to the mean stream function so that $\psi = \bar{\psi} + \mu\psi'$. The difference with subsection 1.1.1 is that the mean flow $\bar{\psi}$ now depends on both x and r to account for the variation of the flow in the x-direction. The resulting linearized vorticity equation for the perturbation ψ' is

$$\frac{\partial}{\partial t}D^2\psi' + \frac{1}{r}\left[\frac{\partial \bar{\psi}}{\partial r}\frac{\partial}{\partial x}D^2\psi' + \frac{\partial \psi'}{\partial r}\frac{\partial}{\partial x}D^2\bar{\psi} - \frac{\partial \bar{\psi}}{\partial x}\frac{\partial}{\partial r}D^2\psi' - \frac{\partial \psi'}{\partial x}\frac{\partial}{\partial r}D^2\bar{\psi}\right]$$
$$+\frac{2}{r^2}\left[\frac{\partial \bar{\psi}}{\partial x}D^2\psi' + \frac{\partial \psi'}{\partial x}D^2\bar{\psi}\right] = 0, \tag{1.14}$$

$$\text{where} \qquad D^2 = \frac{\partial^2}{\partial x^2} + \frac{\partial^2}{\partial r^2} - \frac{1}{r}\frac{\partial}{\partial r}. \tag{1.15}$$

Because the flow is assumed to vary slowly in the x-direction, we introduce the slow scale $X = \epsilon x$ and the mean stream function spatial dependence is then expressed as $\bar{\psi} = \bar{\psi}(r, X)$. To apply the multiple scale method and derive the amplitude evolution equation, we also need to introduce the slow scale $T = \epsilon t$ and and the fast scale $\lambda = \Theta(X,T)/\epsilon$. The stream function perturbation can now be expressed in terms of these variables

$$\psi'(x, r, t, \epsilon) = F(\lambda, r, X, T, \epsilon). \tag{1.16}$$

Applying the chain rule, the partial derivatives become

$$\begin{aligned}
\frac{\partial \psi'}{\partial x} &= \Theta_X\frac{\partial F}{\partial \lambda} + \epsilon\frac{\partial F}{\partial X}, \\
\frac{\partial \psi'}{\partial t} &= \Theta_T\frac{\partial F}{\partial \lambda} + \epsilon\frac{\partial F}{\partial T}, \\
\frac{\partial \psi'}{\partial r} &= \frac{\partial F}{\partial r}.
\end{aligned} \tag{1.17}$$

Expanding F in powers of ϵ gives

$$F = F_0(\lambda, r, X, T) + \epsilon F_1(\lambda, r, X, T) + O(\epsilon^2). \tag{1.18}$$

We are now in a position to substitute F back into (1.14). We can also take advantage of the fact that the mean stream function $\bar{\psi}$ does not depend on the fast variable λ and immediately look for a solution of the form

$$F_0 = \Phi_0(r, X, T)e^{i\lambda}. \tag{1.19}$$

To order ϵ^0 this gives:

$$L(\Phi_0) = 0, \tag{1.20}$$

where

$$L = \left(\frac{\psi_r}{r} + \frac{\Theta_T}{\Theta_X}\right)\left(\left(\frac{\partial^2}{\partial r^2} - \frac{1}{r}\frac{\partial}{\partial r}\right) - \Theta_X^2\right) - \left(\frac{\partial^2}{\partial r^2} - \frac{1}{r}\frac{\partial}{\partial r}\right)\frac{\psi_r}{r}. \tag{1.21}$$

It is worth noting that the equation (1.20) is equivalent to solving the parallel flow problem for an incompressible fluid if Θ_X and $-\Theta_T$ are replaced by α and ω, i.e. the wavenumber and frequency of the perturbation. This amounts to solving (1.8) for the pressure perturbation $\hat{p}$ if the temperature is assumed to be constant and the Mach number is zero. Obviously, the two problems share the same boundary conditions and so in solving (1.20), we require that Φ_0 be bounded as $r \to 0$ and $r \to \infty$. The solution of (1.20) also gives us a relation between Θ_X and Θ_T

$$g(\Theta_X, \Theta_T, X) = 0. \tag{1.22}$$

For a parallel flow, this would be a dispersion relation of the form $\alpha(\omega) = \alpha$ discussed in subsection 1.1.2. Here, however, equation (1.22) is actually a partial differential equation for the unknown phase $\Theta(X, T)$.

The general solution of the perturbation order ϵ^0 is now

$$F_0 = A(X, T)\phi_0(r, X, T)e^{i\lambda}, \tag{1.23}$$

where $A(X,T)$ is a slowly varying amplitude of the wave packet and ϕ_0 is a solution of (1.20). In order to obtain the equation for the amplitude $A(X,T)$, it is necessary to consider what happens at order ϵ. Taking advantage of the fact that $\bar{\psi}$ has no λ dependence, we look for a solution of the form $F_1 = \Phi_1 e^{i\lambda}$. It is important to point out that we have omitted a term proportional to $\lambda\Phi_1 e^{i\lambda}$ in F_1 despite the anticipation of non-homogeneous terms proportional to $e^{i\lambda}$ at this order. The omission of this secular term is justified by the requirement that the asymptotic expansion be uniformly valid as $\epsilon \to 0$. Indeed, F_1 is included in the expansion (1.18) in the form ϵF_1, hence the secular term would be proportional to $\epsilon\lambda\Phi e^{i\lambda}$ which is of order $\epsilon\lambda = O(1)$. This contradicts the validity of the asymptotic expansion and any secular term of this form must be set equal to zero.

With the form of F_1 in mind, the problem, to order ϵ is

$$L(\Phi_1) = K\left(\frac{\partial\Phi_0}{\partial T}\right) + M\left(\frac{\partial\Phi_0}{\partial X}\right) + N\left(\Phi_0\right), \tag{1.24}$$

where the operators K, M, and N are given by:

$$K = -\frac{\partial^2}{\partial r^2} + \frac{1}{r}\frac{\partial}{\partial r} + \Theta_X^2, \tag{1.25}$$

$$M = -\frac{\psi_r}{r}\left(\frac{\partial^2}{\partial r^2} - \frac{1}{r}\frac{\partial}{\partial r}\right) + \left(\frac{3\psi_r\Theta_X^2}{r} - 3\frac{\psi_{rr}}{r^2} + \frac{\psi_{rrr}}{r} + 2\Theta_T\Theta_X + 3\frac{\psi_r}{r^3}\right), \tag{1.26}$$

and

$$\begin{aligned} N = {} & \frac{\psi_X}{r}\frac{\partial^3}{\partial r^3} - 3\frac{\psi_X}{r^2}\frac{\partial^2}{\partial r^2} - \left(\frac{\psi_X\Theta_X^2}{r} + \frac{\psi_{Xrr}}{r} - \frac{\psi_{Xr}}{r^2} - 3\frac{\psi_X}{r^3}\right)\frac{\partial}{\partial r} \\ & + \left(2\frac{\psi_X\Theta_X^2}{r^2} + 3\frac{\psi_r\Theta_X\Theta_{XX}}{r} + \Theta_T\Theta_{XX} + 2\Theta_{TX}\Theta_X\right). \end{aligned} \tag{1.27}$$

For this problem to have a solution, it must satisfy a solvability condition. Taking $\tilde{\phi}$ to be the solution of the adjoint problem of (1.20), this condition is expressed as

$$0 = \int_0^\infty \left[K\left(\frac{\partial\Phi_0}{\partial T}\right) + \left(M\frac{\partial\Phi_0}{\partial X}\right) + N\left(\Phi_0\right)\right]\tilde{\phi}\,dr. \tag{1.28}$$

Because the general form of Φ_0 is given by $\Phi_0 = A(X,T)\phi_0(r,X,T)$, as seen from equations (1.19) and (1.23), the solvability condition yields an equation for the amplitude $A(X,T)$. This equation is

$$k(X,T)\frac{\partial A}{\partial T} + m(X,T)\frac{\partial A}{\partial X} + n(X,T)A = 0, \tag{1.29}$$

where k, m, and n are obtained from the orthogonality condition (1.28). They are given by

$$k(X,T) = \int_0^\infty K(\phi_0)\,\tilde{\phi}dr, \tag{1.30}$$

$$m(X,T) = \int_0^\infty M(\phi_0)\,\tilde{\phi}dr, \tag{1.31}$$

and

$$n(X,T) = \int_0^\infty \left[K\left(\frac{\partial \phi_0}{\partial T}\right) + M\left(\frac{\partial \phi_0}{\partial X}\right) + N(\phi_0)\right]\tilde{\phi}dr. \tag{1.32}$$

At this point, we have derived a non-homogenous equation for a amplitude traveling at the group velocity $c_g(X,T) = -m/k$. What is still missing from equation (1.29) is the dispersive effect of the slowly varying jet on $A(X,T)$, which is one of the main objectives of this derivation. To include this effect, we need to go to higher orders in the multiple scale expansion. To ensure that $A(X,T)$ is separable at the desired order, it is necessary to go back to the beginning and introduce a new variable that travels with the wave packet

$$\zeta = \epsilon^{1/2}\left(t - \int \frac{k(\epsilon x, \epsilon t)}{m(\epsilon x, \epsilon t)}dx\right). \tag{1.33}$$

The rationale behind the definition of ζ will made clear below as the multiple scale expansion is carried out.

With the new dependence on ζ, i.e. $\psi' = F(\lambda, r, X, T, \zeta, \epsilon)$, the partial derivatives become

$$
\begin{aligned}
\frac{\partial \psi'}{\partial x} &= \Theta_X \frac{\partial F}{\partial \lambda} + \epsilon^{1/2} \frac{1}{c_g} \frac{\partial F}{\partial \zeta} + \epsilon \frac{\partial F}{\partial X}, \\
\frac{\partial \psi'}{\partial t} &= \Theta_T \frac{\partial F}{\partial \lambda} + \epsilon^{1/2} \frac{\partial F}{\partial \zeta} + \epsilon \frac{\partial F}{\partial T}, \\
\frac{\partial \psi'}{\partial r} &= \frac{\partial F}{\partial r}.
\end{aligned}
\tag{1.34}
$$

We also need to revise the expansion of F to account for the fact that the new variable is of order $\epsilon^{1/2}$. The new expansion takes the form

$$F = F_0(\lambda, r, X, T, \zeta) + \epsilon^{1/2} F_{1/2}(\lambda, r, X, T, \zeta) + \epsilon F_1(\lambda, r, X, T, \zeta) + O(\epsilon^{3/2}). \tag{1.35}$$

By setting $F_0 = \Phi_0(r, X, T, \zeta)e^{i\lambda}$ once again, we recover (1.20), (1.21), and (1.22) to order ϵ^0. So similarly to (1.23), the general solution takes the form

$$F_0 = A(X, T, \zeta)\phi_0(r, X, T)e^{i\lambda}. \tag{1.36}$$

Things get a little more interesting at order $\epsilon^{1/2}$. Just as before, we look for a solution of the form $F_{1/2} = \Phi_{1/2}(r, X, T, \zeta)e^{i\lambda}$, where the secular term of the form $\lambda\phi_0$ has been set to zero in order to satisfy the requirement that the expansion be uniformly valid as $\epsilon \to 0$. We obtain an non-homogeneous equation analogous to (1.24) with the important addition that the non-homogeneous terms are all multiplied by $\frac{\partial A}{\partial \zeta}$

$$L(\Phi_{1/2}) = \left(K(\phi_0) + \frac{1}{c_g} M(\phi_0) \right) \frac{\partial A}{\partial \zeta}. \tag{1.37}$$

The homogeneous solution of equation (1.37) is $A_{1/2}\phi_0$, where $L(\phi_0) = 0$ and $A_{1/2}(X, T, \zeta)$ is an unknown amplitude determined at order $\epsilon^{3/2}$. The particular solution is obtained by variation of parameters and has the form $\frac{\partial A}{\partial \zeta}\phi_{1/2}(r, X, T)$. Hence, the general solution at order $\epsilon^{1/2}$ is given by

$$F_{1/2} = \left(\frac{\partial A}{\partial \zeta}\phi_{1/2} + A_{1/2}\phi_0 \right) e^{i\lambda}. \tag{1.38}$$

However, for there to be such a solution, it is necessary for the non-homogeneous part of (1.37) to satisfy the solvability condition

$$0 = \int_0^\infty \left[K(\phi_0) + \frac{1}{c_g} M(\phi_0) \right] \tilde{\phi} dr = k + \frac{1}{c_g} m \,, \tag{1.39}$$

where $\tilde{\phi}$ is again the solution of the adjoint problem of (1.20). Because the group velocity is given $c_g = -m/k$, the two terms in (1.39) cancel and the solvability condition is automatically satisfied. It is precisely for this cancellation to take place that ζ was defined by (1.33).

Finally, order ϵ allows us to obtain the amplitude evolution equation we are seeking. Taking the solution at this order to have the form $F_1 = \Phi_1 e^{i\lambda}$, once more omitting the secular term in the process, leads to

$$L(\Phi_1) = G\left(\frac{\partial \Phi_{1/2}}{\partial \zeta}\right) - iQ(\Phi_0) + P(\frac{\partial^2 \Phi_0}{\partial \zeta^2}), \tag{1.40}$$

where

$$G = K + \frac{1}{c_g} M, \tag{1.41}$$

the same non-homogeneous operator as in equation (1.37). Q has already been derived from order ϵ in equation (1.24):

$$Q = K\frac{\partial}{\partial T} + M\frac{\partial}{\partial X} + N. \tag{1.42}$$

As for P, it is a new operator

$$P = -\frac{1}{c_g}\left(2\Theta_X + \frac{\Theta_T}{c_g} + 3\frac{\psi_r \Theta_X}{c_g r}\right). \tag{1.43}$$

The forms of G and Q are not too surprising in retrospect. The non-homogeneous terms of equation (1.40) must either come from the contribution of $\epsilon^{1/2} \cdot \epsilon^{1/2} = \epsilon$, which gives G and P, or the contributions from ϵ, which gives Q.

Applying the solvability condition to equation (1.40) means that

$$0 = \int_0^\infty \left[G\left(\frac{\partial \Phi_{1/2}}{\partial \zeta}\right) - iQ(\Phi_0) + P\left(\frac{\partial^2 \Phi_0}{\partial \zeta^2}\right)\right] \tilde{\phi} dr. \tag{1.44}$$

Substituting $\Phi_0 = A\phi_0$ and $\Phi_{1/2} = \frac{\partial A}{\partial \zeta}\phi_{1/2} + A_{1/2}\phi_0$ from equations (1.36) and (1.38) gives

$$0 = i\int_0^\infty \left[G\left(\phi_{1/2}\right) + P(\phi_0)\right] \frac{\partial^2 A}{\partial \zeta^2}\tilde{\phi} dr + \int_0^\infty Q(\Phi_0)\tilde{\phi} dr \,, \tag{1.45}$$

where we made use of the fact that $\int_0^\infty G(\phi_0)\tilde{\phi} dr = 0$ as shown in equation (1.39). Noting that $\int_0^\infty Q(\Phi_0)\tilde{\phi} dr$ is simply the left hand side of equation (1.28), we have derived the desired amplitude evolution equation, namely,

$$k(X,T)\frac{\partial A}{\partial T} + m(X,T)\frac{\partial A}{\partial X} + p(X,T)\frac{\partial^2 A}{\partial \zeta^2} + n(X,T)A = 0, \tag{1.46}$$

where

$$p(X,T) = i\int_0^\infty \left[G\left(\phi_{1/2}\right) + P(\phi_0)\right] \frac{\partial^2 A}{\partial \zeta^2}\tilde{\phi} dr, \tag{1.47}$$

and k, m, and n are defined by equations (1.30), (1.31), and (1.32). This equation is very similar to (1.29), as can be expected, but this time it includes the dispersive effect of the medium on the wave through the term $p\frac{\partial^2 A}{\partial \zeta^2}$.

Chapter 2

Description of the Numerical Problem

2.1 Mean Flow Profiles

As stated in the introduction, we wish to investigate the stability of compressible mean flows representative of those in the experiments reported by Papamoschou [19]. In modelling these profiles, we have adapted to some extent ideas employed by other investigators, such as Crighton and Gaster [5], with modifications so as to describe a coaxial jet. The first velocity profile that we employ, hereafter referred to as profile 1, has the form

$$\begin{aligned} \bar{u} &= (1-h)\bar{u}_1 + h\bar{u}_2, \\ \text{where } u_n &= \frac{1}{2}\left\{1+\tanh\left[b_n\left(\frac{R_n}{r}-\frac{r}{R_n}\right)\right]\right\}, \text{ and } \quad n=1,2\,. \end{aligned} \tag{2.1}$$

The parameter h is the velocity ratio, U_s/U_p in the notation of Ref. [19], of the secondary (bypass) stream to the primary stream of the coaxial jet (see Fig. 2.1). R_1 and R_2 represent the radii of the primary and secondary streams, respectively. The radii are defined such that they coincide with the mid-point of the velocity in the two streams. In (2.1) this corresponds to $\bar{u}_1(R_1) = \bar{u}_1(0)/2$ and $\bar{u}_2(R_2) = \bar{u}_2(0)/2$. We, in fact, use R_1 as the reference length scale for the problem; hence, the velocity profile $\bar{u}$ is normalized so that $R_1 = 1$. Finally, the parameters b_1 and b_2 are related to the momentum thicknesses θ_1 and θ_2, i.e. the momentum thickness computed for $\bar{u}_1$ and $\bar{u}_2$ independently, through $b_n = R_n/4\theta_n$. For incompressible plane flows normalized at $r = 0$, as is the case here, the momentum thickness is defined as

$$\theta = \int_0^\infty u\,(1-u)\;dr\,. \tag{2.2}$$

For a thin shear layer, such as the shear layers considered here, equation (2.2) is a good approximation of the momentum thickness. In fact, (2.2) is regularly used in the study of axisymmetric flows instabilities [5, 16, 22].

As already mentioned, we compute two separate momentum thicknesses instead of just one for $\bar{u}$. The reason that we employ two momentum thicknesses is that each of the two instability modes appears to be associated with one or the other of the mixing layers. We are following here the procedure of Talamelli and Gavarini [22], who investigated the stability of incompressible coaxial jets to axisymmetric perturbations. Finally, we note that, at the Mach numbers under consideration, it is the velocity profile that most influences the stability, so the incompressible momentum thickness is sufficient for the purpose at hand.

Turning now to the temperature profile, the "cold" temperature profile $\bar{T}_2$ is taken from Papamoschou's experiments, while the "hot" temperature profile $\bar{T}_1$ is taken from the mean flow of a typical turbofan engine such as the General Electric CFM56, for which the primary stream is heated. To relate the temperature profiles to the velocity profile, a method commonly employed is the Crocco-Busemann law [21]

$$\bar{T}(r) = \bar{T}_\infty + \left(1 - \bar{T}_\infty\right)\bar{u}(r) + \frac{(\gamma-1)\,M_0^2\bar{u}\,(1-\bar{u})}{2}\,. \tag{2.3}$$

Having obtained the values of the "cold" temperature profile $\bar{T}_2$ of the primary stream, secondary stream and outer region directly from Papamoschou, we did not need to use the Busemann-Crocco law. However, in order to allow for the temperature to vary smoothly between the streams, we were inspired by (2.3) to use a quadratic relation between $\bar{T}_2$ and $\bar{u}$

$$\bar{T}_2 = a\bar{u}^2 + b\bar{u} + c\,. \tag{2.4}$$

Using Papamoschou's data, the constants for a temperature profile normalized at $r = 0$ were found to be $a = -0.0592$, $b = -0.1032$ and $c = 1.1624$. As for the hot temperature profile $\bar{T}_1$, Papamoschou advised us to use

$$\bar{T}_1 = \frac{1}{2}\left\{1 + \tanh\left[b_1\left(\frac{R_n 1}{r} - \frac{r}{R_1}\right)\right]\right\} + \frac{1}{2}. \tag{2.5}$$

The distinctive feature of T_1 is that the temperature of the primary stream, where the flow is heated by combustion, is twice that of the secondary stream and the outer region. Fig. 2.1 shows the velocity profile 1 and the temperature profiles, all of which are normalized at $r = 0$. Finally, the Mach number for $\bar{T}_1$ is $M_0 = 0.6558$, while the Mach number for $\bar{T}_2$ is $M_0 = 1$.

A primary subject of interest for this thesis is the effect of the radius ratio $\Gamma = R_2/R_1$ on the stability of the jet. From Eq. (2.1), it is straightforward to vary Γ by changing R_2. However, to do this without also changing b_2 does not account for the change in the momentum thickness θ_2 of the outer mixing layer as Γ varies. For a two-dimensional profile, no such change would occur since changing Γ corresponds simply to a translation of the shear layer. However, the axisymmetric case is not as straightforward, because a simple translation would be inconsistent with the cylindrical geometry of the problem. To account for this change in the momentum thickness of the outer stream, θ_2, we employ the relation

$$\theta = \frac{3}{100}\left(x + \frac{2}{3}D\right) \tag{2.6}$$

based on similarity arguments for axisymmetric jets first used by Crighton and Gaster [5] in the context of slowly diverging jet flows. When applied to a coaxial

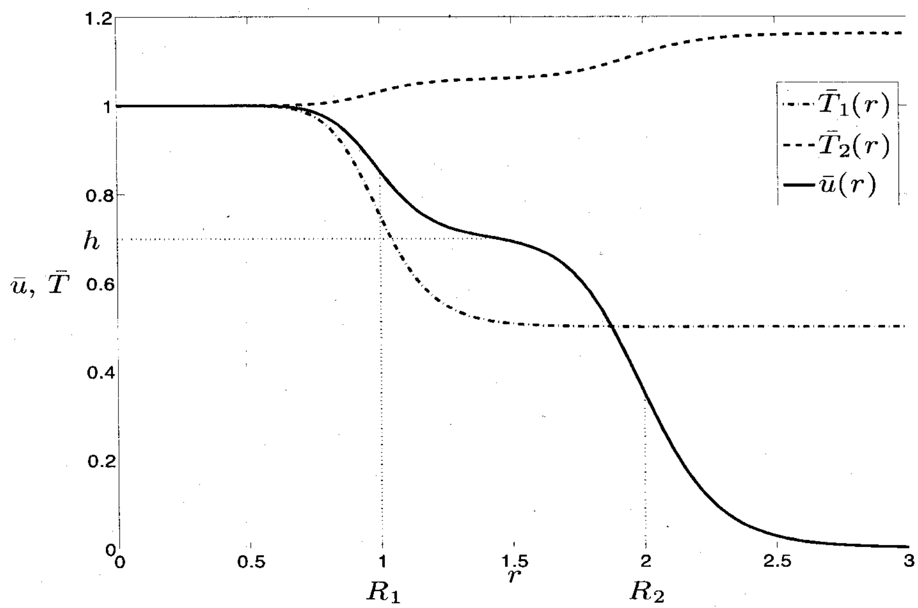

Figure 2.1: Velocity defined by equation (2.1) along with hot and cold temperature profiles. The velocity ratio used for this figure is $h = 0.7$, the radius ratio is $\Gamma = 2$, and the momentum thicknesses are $\theta_1 = 0.1$ and $\theta_2 = 0.14$.

jet profile, this relation was found to be an excellent representation of Papamoschou's experimental data for the first ten primary radii, R_1, after the exhaust (see Fig. 13 (b) of Ref. [19]).

According to Crow and Champagne [6], the instabilities first develop one diameter length away from the exhaust of the jet. Using this as the axial position of the profile, the two momentum thicknesses are $\theta_1 = 0.1$ and $\theta_2 = 3/50 + R_2/25$. Using Papamoschou's Fig. 13 (b) again, the reference geometry for this thesis (Fig. 2.1) has velocity ratio $h = 0.7$ and radius ratio $\Gamma = 2$. The secondary stream momentum thickness for this geometry is therefore $\theta_2 = 0.14$.

We also considered a second approach to account for the relation between Γ and

θ_2. Going back to the boundary layer equations, we found that Schlichting's [21] similarity solution could be adapted to describe the shape of the secondary stream by matching it to the primary stream. Specifying R_2 in this new profile, hereafter referred to as profile 2, automatically determines the secondary stream thickness θ_2, hence providing for a simple way of varying the radius ratio Γ. Profiles 1 and 2 are compared in Fig. 2.2. For a derivation of profile 2, we refer the reader to the Appendix.

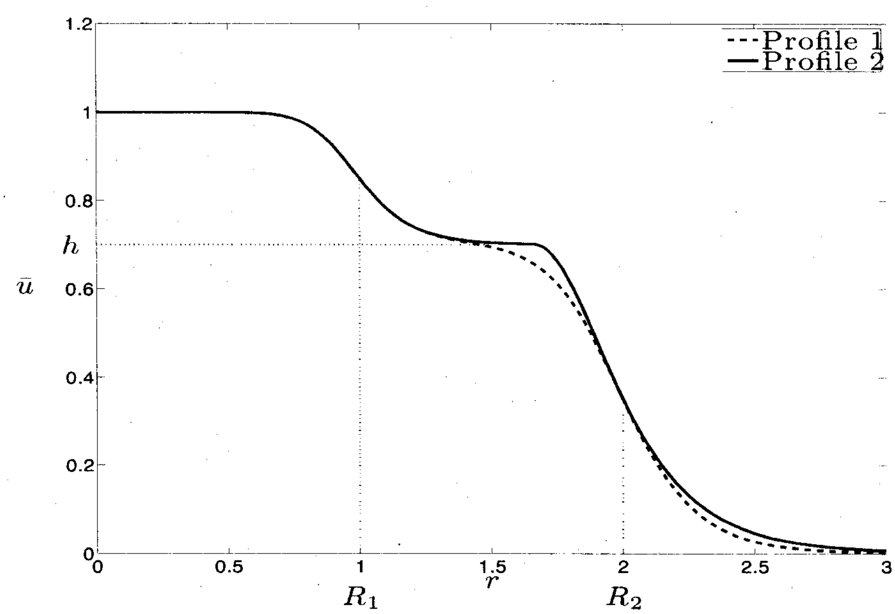

Figure 2.2: Comparison of velocity profile 1 from equation (2.1) and the velocity profile 2 using the matched similarity solution as described in the appendix, equation. The velocity ratio used for this figure is $h = 0.7$, the radius ratio is $\Gamma = 2$, and the momentum thicknesses are $\theta_1 = 0.1$ and $\theta_2 = 0.14$.

2.2 Numerical Method

The range of integration is from $r = 0$ to $r \to \infty$ and, because the governing equation for the pressure perturbation (1.8) has a regular singular point at $r = 0$ and an irregular singular point at infinity, series solutions are required at both ends. A Runge-Kutta method was used to carry out the integration. For neutral or for unstable perturbations with small growth rates, it is necessary to indent the integration contour to avoid the singularity at $\bar{u}_c - \omega/\alpha = 0$ in order to obtain accurate converged solutions. Because $\bar{u}'_c$ is negative, the integration path passes above the singularity in the complex r plane, corresponding to the viscous limit as the Reynolds number $Re \to \infty$ or to the initial value problem as $t \to \infty$ (see Ref. [14], p.124 for the two dimensional case). The integration path used is shown in Fig. 2.3.

We first take a look at the infinite series used to deal with the singular points at $r = 0$ and $r = \infty$. Near the origin, i.e. $r \to 0$, equation (1.8) reduces to

$$\frac{d^2\hat{p}}{dr^2} + \frac{1}{r}\frac{d\hat{p}}{dr} - \left[\alpha^2\left(1 - M_0^2 H\right) + \frac{m^2}{r^2}\right]\hat{p} = 0\,. \tag{2.7}$$

The solution to (2.7) can be represented by a Frobenius expansion having the form

$$\hat{p} = p_0\, r^{|m|}\,\left[1 + \zeta_1 r^2 + O(r^4)\right]. \tag{2.8}$$

If the velocity and temperature profiles are relatively flat near the centerline, as in our case, $H(r) \simeq H(0)$ and a good approximation to the solution is given by the modified Bessel function I_m so that near $r = 0$

$$\hat{p} \simeq I_m\left(\alpha\sqrt{1 - M_0^2 H(0)}\, r\right)\,. \tag{2.9}$$

As $r \to \infty$, $\bar{u} \to 0$ and H is constant, such that once again, (1.8) becomes a modified Bessel equation. This time, however, the desired behavior corresponds to the function K_m, whose asymptotic expansion decays exponentially as $r \to \infty$ so that

$$\hat{p} \sim K_m\left(\alpha\sqrt{1 - M_0^2 H(\infty)}\, r\right)\,. \tag{2.10}$$

Using the conditions (2.9) and (2.10) above to initiate the integration, we integrate toward an interior value of r from either side and compute the Wronskian $W(\omega,\alpha)$ of the two solutions at this interior point. Integrating toward an interior point means that the Runge-Kutta method will not pick up the exponentially growing solutions as $r \to 0$ or $r \to \infty$. Iterating on the parameters of the problem, the integration is repeated until $W(\omega,\alpha) = 0$. The Newton method for complex functions was used in order to achieve a rapid convergence. Because this algorithm is quite sensitive to initial conditions, a good starting guess was first obtained by plotting W on a coarse grid. Once the Newton method had successfully converged, it was simple to reuse the solutions as subsequent guesses by varying the parameters of interest by small increments.

Indenting the integration path into the complex plane to solve equation 1.8 also requires some explanation. In the interest of simplicity, we use a general second order equation

$$f\left(\frac{d^2\hat{p}}{dr^2}, \frac{d\hat{p}}{dr}, \hat{p}, r\right) = 0. \tag{2.11}$$

With the complex variable $r = r_r + ir_i$, the first derivative takes the form

$$\frac{d\hat{p}}{dr} = \left(\frac{\partial r_r}{\partial r}\right)\frac{d\hat{p}}{dr_r} + \left(\frac{\partial r_i}{\partial r}\right)\frac{d\hat{p}}{dr_i}\,. \tag{2.12}$$

On the segment from 0 to A in Fig. 2.3, the independent variable is $r_r = r$ and so (2.11) is the same, except for the obvious substitution. On the segment from A to B however, the independent variable r_i is given $r = r_A + ir_i$, where r_A is the real component of point A. Isolating for r_i we get $r_i = -i(r - r_A)$ and so the equation (2.12) reduces to

$$\frac{d\hat{p}}{dr} = -i\frac{d\hat{p}}{dr_i}\,, \tag{2.13}$$

while the second order derivative becomes

$$\frac{d^2\hat{p}}{dr^2} = (-i)^2\frac{d\hat{p}}{dr_i^2} = -\frac{d\hat{p}}{dr_i^2}\,. \tag{2.14}$$

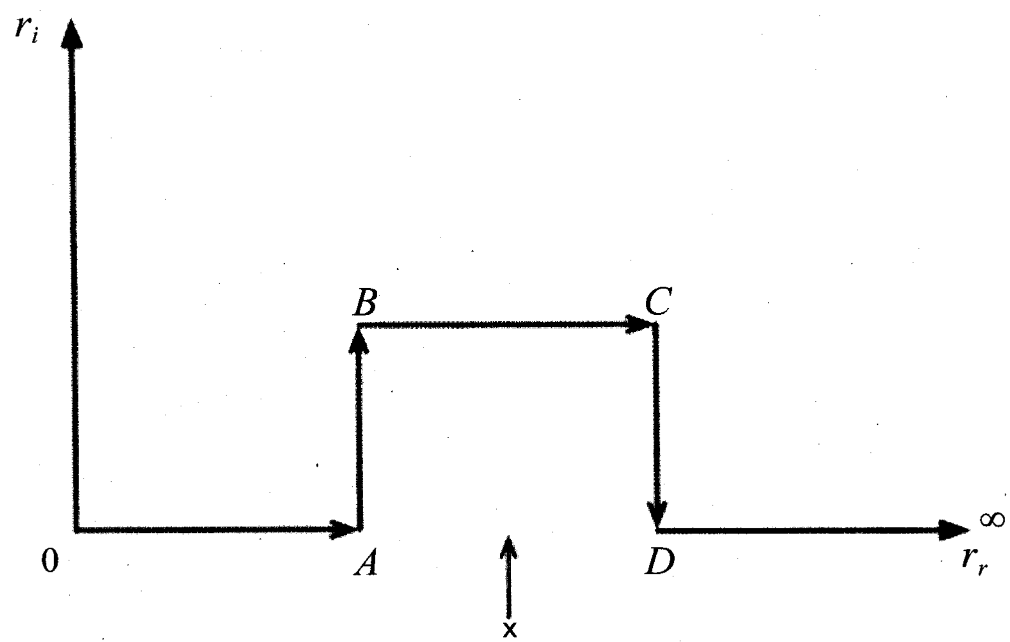

Figure 2.3: Integration path for $\hat{p}$ in equation (1.8). The indented contour is used in order to avoid the singularity at $\bar{u}_c - \omega/\alpha = 0$, denoted by "x" in the figure, as the growth rate approaches the neutral solution, i.e. $-\alpha_i \rightarrow 0$.

This means that equation (2.11) now has the form

$$f\left(-\frac{d^2\hat{p}}{dr_i^2}, -i\frac{d\hat{p}}{dr_i}, \hat{p}, r_A + ir_i\right) = 0\,, \tag{2.15}$$

with r_i as the independent variable. Using the same technique, it is straightforward to find what form (2.11) takes along any of the segments of Fig. 2.3.

It is not sufficient to know the form of the equation along each segment to solve it, however. The boundary conditions at each point must also be modified in order for the integration to be correctly performed. Taking point A as an example again, we must relate the values obtained by integrating from $0 \rightarrow A$ to the boundary conditions needed to integrate along $A \rightarrow B$. For a second order equation such as (2.11), the necessary boundary conditions are $\hat{p}$ and $\frac{d\hat{p}}{dr}$. Using the equation (2.12) once more, we have

$$\frac{d\hat{p}}{dr} = \frac{d\hat{p}}{dr_r}, \quad \text{and} \quad \frac{d\hat{p}}{dr} = -i\frac{d\hat{p}}{dr_i} \tag{2.16}$$

along the segment from 0 to A and from A to B respectively. In other words, the derivative with respect to r_r and r_i at point A are related by

$$\frac{d\hat{p}}{dr_r} = i\frac{d\hat{p}}{dr_i} . \tag{2.17}$$

Using this relation, it is easy to convert the solution obtained by integrating from 0 to A into the boundary conditions for the segment from A to B. Because all the segments intersect at a 90° angle, this relation holds for all the other points in Fig. 2.3.

As a final note on the indented path, one has to be mindful of matched profiles such as profile 2 described in the Appendix. In the specific case of profile 2, the indented path cannot include the matching point, which is really a line in the complex plane. The problem is that Profile 2 is not analytic across this line. Hence, it does not make sense to integrate accross this line, except on the real axis where the matching guarantees a continuous first derivative. In practice, avoiding this problem should not present significant difficulties if the indented path is kept relatively short.

It is worth mentioning, before moving on to the computational results, that our implementation of the numerical method described in this section was tested using Michalke's results such as Fig.9 of his survey article [16]. As expected, we were able to reproduce is results without problems.

Chapter 3

Computational Results

The necessary conditions for instability of the incompressible axisymmetric problem given in subsection 1.1.2 specify that there are at most two unstable modes per azimuthal wavenumber m when applied to profiles 1 and 2, discussed above. Both of these modes were found to be unstable for the first few wavenumbers, $m = 0$, 1, and 2. The result, discussed in subsection 1.1.2, that the neutral solution of these modes must satisfy $\bar{u} = \omega/\alpha$ for r such $Q'(r) = 0$ (see Eq. (1.10)), can be used to identify the modes. One value of r for which $\bar{u} = \omega/\alpha$ is found to lie in the primary stream, while the other one is found to lie in the secondary stream. For this reason, the modes will be referred to as mode I and mode II, depending on whether their neutral limit lies in the primary or secondary stream.

3.1 Two-dimensional vs Axisymmetric Incompressible Jet Flows

The mirror symmetry about the x-axis for two-dimensional jets means that there are even and odd modes. Applying the two-dimensional criteria for instability, inflection

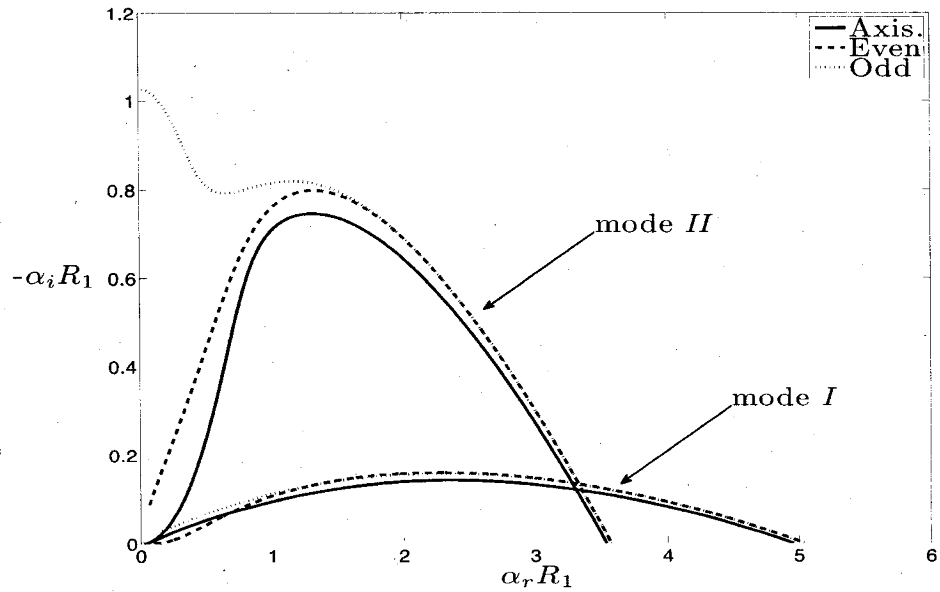

Figure 3.1: Growth rates $-\alpha_i$ of the two-dimensional modes and axisymmetric modes with $m = 0$ for the incompressible profile 1 with velocity ratio $h = 0.7$ and radius ratio $\Gamma = 2$.

point of maximum vorticity, to profile 1 suggests that there are two even and two odd modes. As in the case of the axisymmetric flow, the modes are associated with the primary stream or the secondary stream. Hence, for two dimensional geometry it still makes sense to refer to modes I and II, provided the symmetry of the mode is specified.

The incompressible instabilities of profile 1 for a two-dimensional and an axisymmetric geometry with $m = 0$ exhibit surprisingly close values of growth rate $-\alpha_i$ for velocity ratio $h = 0.7$ and radius ratio $\Gamma = 2$. Nevertheless, Fig. 3.1 shows that the two-dimensional modes are slightly more unstable than the axisymmetric modes, while the phase speed c_{ph} is greater for the axisymmetric modes, see Fig.3.2. The

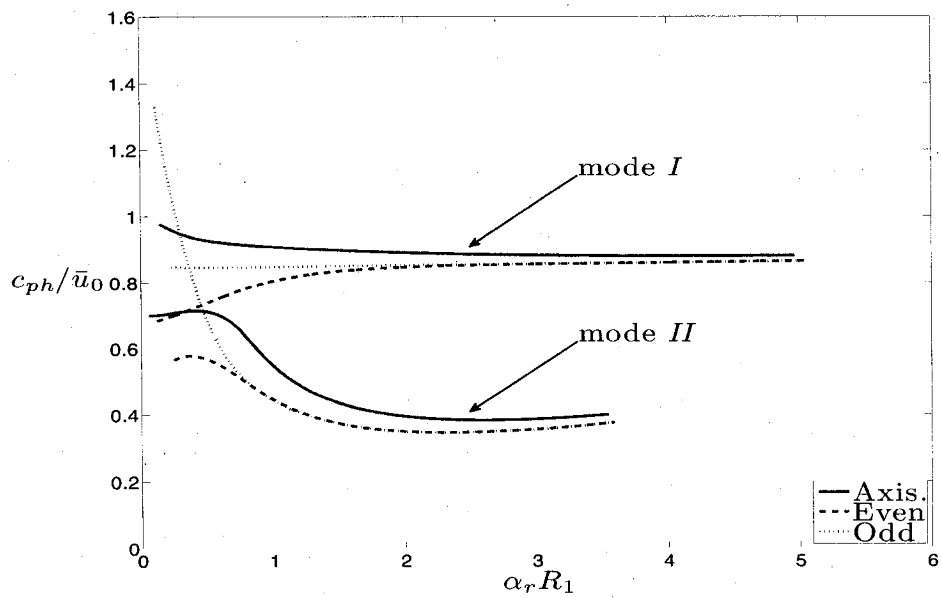

Figure 3.2: Phase speed c_{ph} of the two-dimensional modes and axisymmetric modes with $m = 0$ for the incompressible profile 1 with velocity ratio $h = 0.7$ and radius ratio $\Gamma = 2$.

exception to this is the phase speed of the odd mode I which becomes infinite as $\alpha_r \to 0$. This mode behaves as an irregular mode, to use Michalke's terminology [16], for small values of α_r. According to Michalke, irregular modes are characterized as having finite growth rate $-\alpha_i > 0$ when $\alpha_r \to 0$, just as in Fig. 3.1. However, for larger values of α_r, this mode still behaves like a regular mode as it tends to a neutral solution. This pinching of a regular and irregular mode is associated with the onset of absolute instability explained by Huerre and Monkewitz [10]. It is worth noting that this behavior of the odd mode I was also found to be present for a two-dimensional broken line profile having the same velocity and radius ratios.

There are two other important differences between the two-dimensional and axisymmetric flows. The first, which has already been mentioned in the introduction, is that there can be many more unstable modes for the axisymmetric jet because of the azimuthal number. Here the $m = 0$ case was used for a comparison with the two-dimensional jet instabilities because, as presented in section 3.3 below, this corresponds to the most unstable case for all the profiles studied here.

The second important difference is that a change in the geometry of the profile will not have the same effect on the two-dimensional modes as on the axisymmetric modes. For instance, the two-dimensional modes are much more affected by a change in the diameter ratio in (2.1). If Γ is increased to 3, the instabilities decrease, as discussed below in section 3.4. This decrease is much more pronounced for the two-dimensional modes, however, to the point where they are no longer the most unstable modes for $\Gamma = 3$.

3.2 Compressible Axisymmetric Jet Flows

Adding compressibility to the problem does not significantly affect the stability of the jet flow. In fact, it is only for mode II, as shown in Fig. 3.3, that there are noticeable differences between the incompressible and the compressible profiles. Interestingly, the incompressible profile is found to be more unstable than the compressible profile, except for the hot profile at low wavenumber α_r. As such, compressibility has a stabilizing effect for both hot and cold profiles. This means that the incompressible stability analysis gives an upper boundary for the most unstable wavenumber, as well as the shape and width of the unstable spectrum.

Nonetheless, the study of the compressible profile is an important problem. Under certain circumstances, it can lead to radiating modes, also referred to as Mach waves by Michalke [16]. These occur when the pressure perturbation $p(r)$ from (1.8) decays as $r^{-1/2}$ rather than exponentially. More specifically, as $r \to \infty$, the pressure

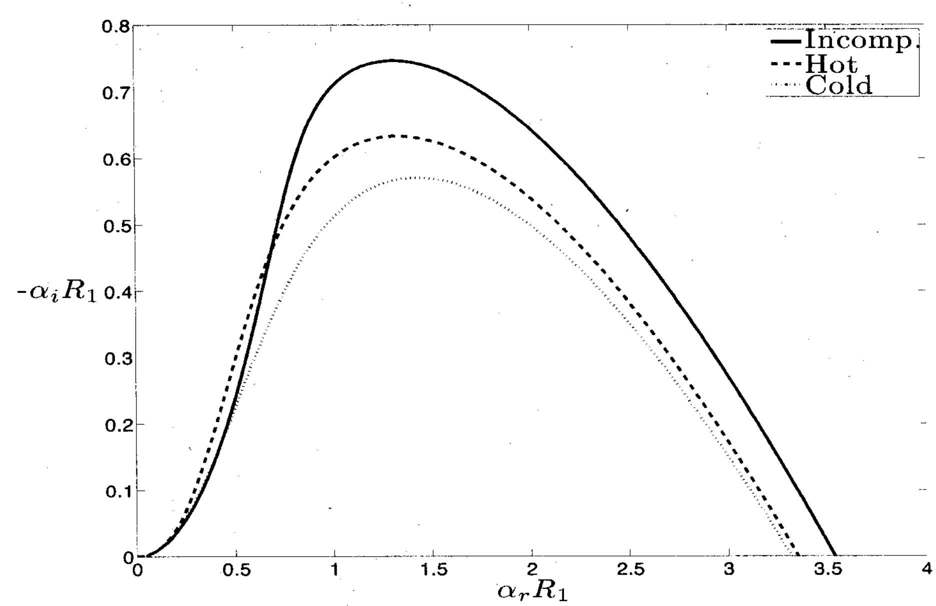

Figure 3.3: Growth rate $-\alpha_i$ of mode II for the incompressible and compressible profile 1 with velocity ratio $h = 0.7$ and radius ratio $\Gamma = 2$.

perturbation behaves according to (2.10), which has the asymptotic form

$$p \sim \frac{1}{\sqrt{r}} e^{(-\lambda_r r - \alpha_i x)} e^{i(\alpha_r x - \lambda_i r + m\phi - \omega t)},$$

$$\text{where} \quad \lambda_r + i\lambda_i = \alpha_r \left(1 - M_c^2 - (k)^2 - i2k\right)^{1/2}, \text{ and } \quad k = -\alpha_i/\alpha_r\,. \qquad (3.1)$$

Hence, radiating modes require that $\lambda_r = 0$. This can happen only for neutral solutions, i.e. $\alpha_i = 0$, and only if the convective wave number, defined as $M_c = (c_{ph}/U_0)M_0(T_0/T_\infty)^{1/2}$, is greater than one. As mentioned by Michalke [16], for $m = 0$ it is easy to determine the wave fronts of the general instability waves from equation (3.1): they are characterized by $\alpha_r x - \lambda_i r - \omega t = constant$. Because instability waves are monochromatic, they will travel in the direction normal to the wave fronts.

Taking the jet axis as reference, the waves's inclination angle μ is given by

$$\cos^2 \mu = \left[1 + \frac{\left(\sqrt{\left(M_c^2 - 1 + k^2\right)^2 + 4k^2} + M_c^2 - 1 + k^2 \right)}{2} \right]^{-1}, \tag{3.2}$$

In the case of radiating modes, we have already established that $\alpha_i = 0$, so the above equation simplifies to

$$\cos \mu = \frac{1}{M_c}. \tag{3.3}$$

Since the propagation speed of the instability waves is given by

$$c_w = a_\infty M_c \cos \mu, \tag{3.4}$$

where a_∞ is the ambient sound speed, radiating modes travel precisely at Mach 1, $\frac{c_w}{a_\infty} = 1$. Hence, these modes correspond to acoustic radiation.

For the temperature profiles studied here, no such radiating modes are observed. However, raising the Mach number for the hot profile does produce a radiating mode. Indeed, using profile 1 from Fig. 2.1 with $h = 0.7$ and $\Gamma = 2$, the above conditions are satisfied for the neutral solution of mode I if $M_0 > 0.8281$. Raising the Mach number is not the only trigger for the development of radiating modes. As will be discussed in section 3.4, increasing the velocity ratio h increases the phase speed c_{ph}, which implies that the Mach number for which a radiating mode develops is lowered. For instance, when h is raised to 0.8, the Mach number at which a radiating mode develops is lowered to 0.7843. Nevertheless, raising h to 1 still does not produce a radiating mode for the reference Mach number for the hot profile ($M_0 = 0.6558$).

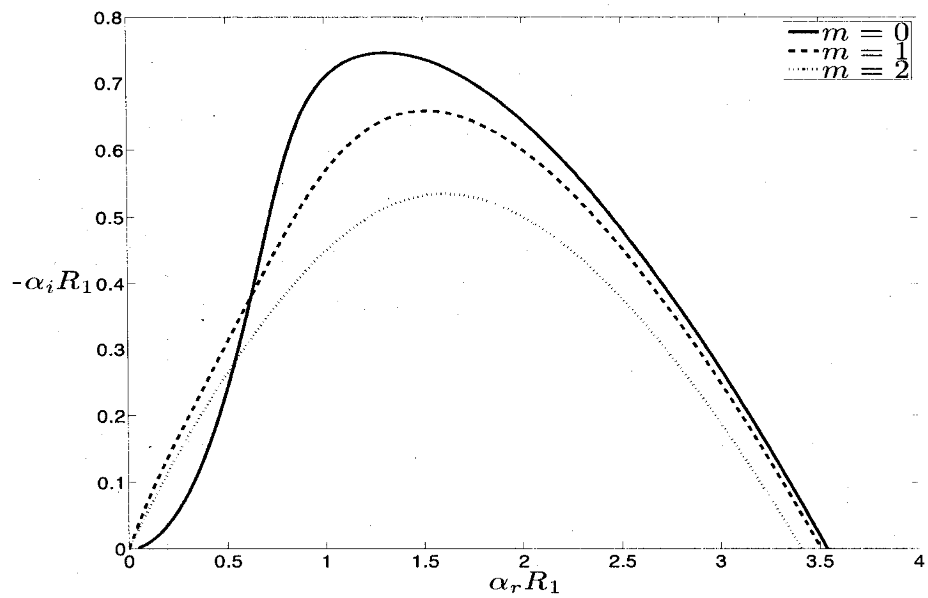

Figure 3.4: Effect of the azimuthal wavenumber m on the growth rate $-\alpha_i$ of mode II for the incompressible profile 1 with velocity ratio $h = 0.7$ and radius ratio $\Gamma = 2$.

3.3 Effect of the Azimuthal Number on Incompressible Jet Flows

The most unstable modes for profile 1 (Fig. 2.1) are found to be the axisymmetric modes for which $m = 0$. The one exception is mode II for a small wavenumber, where both $m = 1$ and 2 are more unstable (see Fig. 3.4). The fact that $m = 0$ is the most unstable mode is in contrast with the profile (1.11), which is only unstable for $m = 1$. As Batchelor and Gill noted, however, the latter result is characteristic of profiles that vary slowly in r, which is not the case here. In fact, Michalke found that for a profile defined only through $\bar{u}_1$ from equation (2.1), the axisymmetric mode is generally more unstable than the $m = 1$ mode.

Michalke conjectured that the important parameter here is θ/R. He found that if $\theta/R > 0.1$, then $m = 1$ becomes more unstable than $m = 0$. This is consistent with Batchelor and Gill's note about slowly varying profiles, as θ/R is inversely proportional to the steepness of the profile when using $\bar{u}_1$.

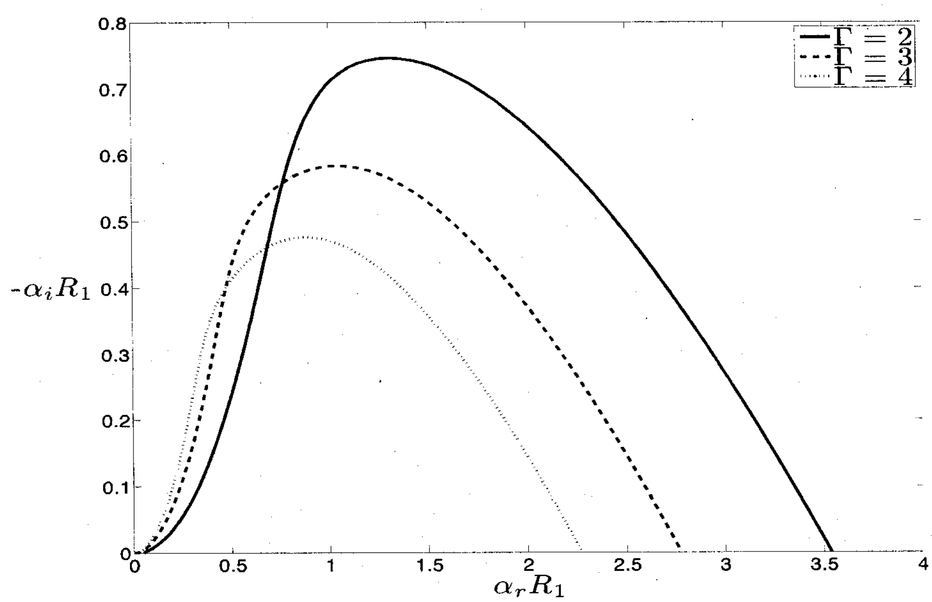

Figure 3.5: Effect of the diameter ratio Γ on the growth rate $-\alpha_i$ of mode II for the incompressible profile 1 with velocity ratio $h = 0.7$.

Michalke's result cannot be transposed directly to coaxial jets. The reference length scale being R_1, there are three relevant parameters: θ_1/R_1, θ_2/R_1, and Γ. As will be shown in section 3.4, mode I is relatively unaffected by θ_2/R_1 and Γ. As such, θ_1/R_1 remains a good criterion to determine which azimuthal wavenumber between $m = 0$ and 1 is the most unstable. In fact, it is for $\theta_1/R_1 = 0.1$, just as for Michalke, that $m = 0$ and $m = 1$ are found to be equally unstable, while higher values are m are less unstable.

For mode II, the transition between $m = 0$ and $m = 1$ as the most unstable azimuthal wavenumber depends on both θ_2/R_1 and Γ. Discarding (2.6) to let Γ and θ_2 vary independently, the transition for $\Gamma = 2$ occurs at $\theta_2/R_1 = 0.246$, while for $\Gamma = 3$, the transition occurs at $\theta_2/R_1 = 0.425$. Finally, if (2.6) is employed, $m = 0$ is more unstable than $m = 1$ for all values of Γ.

3.4 Effect of Velocity and Radius Ratios on Incompressible Jet Flows

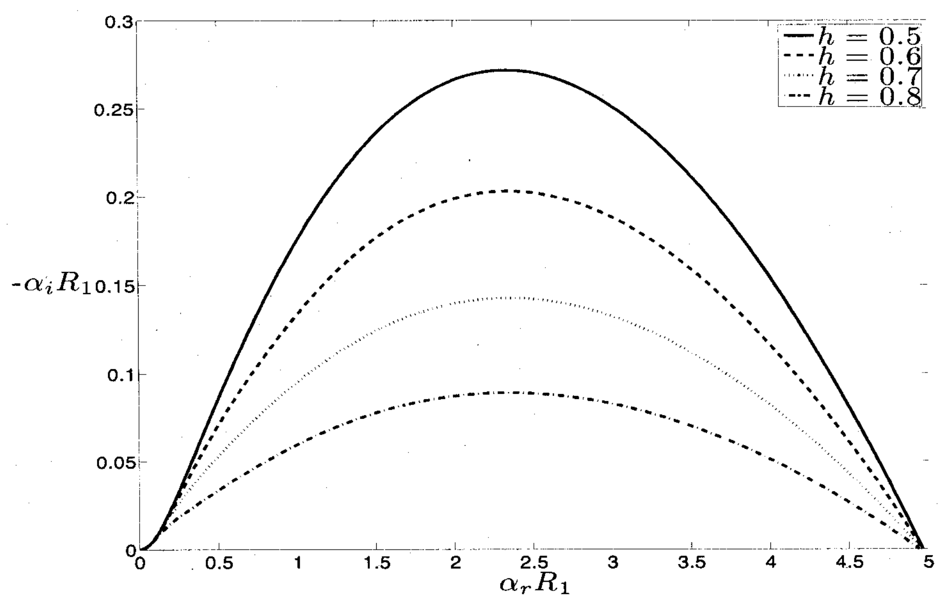

Figure 3.6: Effect of the velocity ratio h on the growth rate $-\alpha_i$ of mode I for the incompressible profile 1 with radius ratio $\Gamma = 2$.

The first striking result arising from the study of the effect of h and Γ on the stability of the coaxial jet is that mode I and II appear to be "independent". By

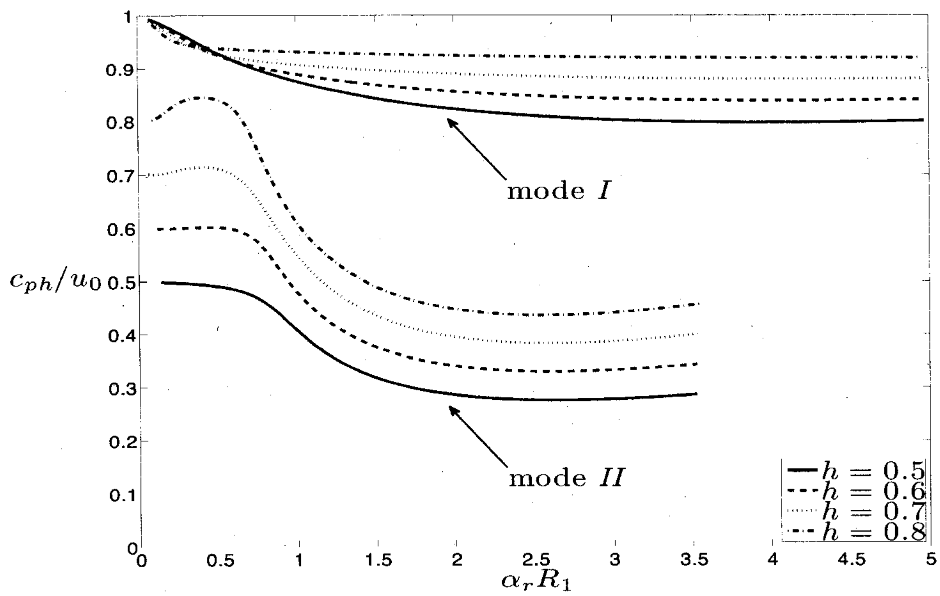

Figure 3.7: Effect of the velocity ratio h on the phase speed c_{ph} of modes I and II for the incompressible profile 1.

this we mean that changing h affects mode I, while changing Γ affects mode II (see Fig. 3.5 and 3.6). In other words, there is a simple mechanism by which one can tune the stability of the two modes. For example, increasing Γ reduces the instability of secondary mode which, in the present case, is the most unstable mode.

However, it would be inexact to claim that all aspects of the two modes can be controlled independently through h and Γ. Looking at the phase speed, Fig. 3.7, it is clear that mode II is affected by a change in h since $c_{ph} \to h$ as $\alpha_r \to 0$ for that mode. A change in Γ, on the other hand, still has little impact on the phase speed or growth rate of mode I provided $\Gamma \geq 2$. As $\Gamma \to 1$ however, the distinction between the two streams is blurred and the stability of the coaxial jet no longer behaves so elegantly. Changes in Γ or h will then affect both modes. Nonetheless, for the values

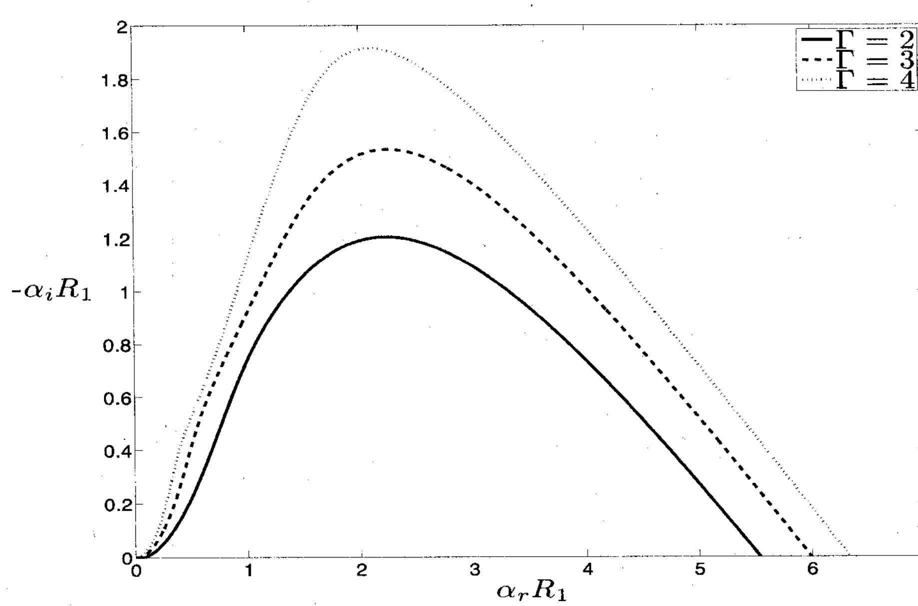

Figure 3.8: Effect of the diameter ratio Γ on the growth rate $-\alpha_i$ of mode II for the incompressible profile 2 with velocity ratio $h = 0.7$.

of interest, Γ does not affect mode I, while h has a limited effect on mode II.

Despite the simplicity of the mechanism described above, changing the radius ratio R_2 is not a straightforward matter, as was touched upon in section 2.1. Ultimately, it was decided to use the relation (2.6) to describe the change in the momentum thickness θ_2 with Γ. However, if the secondary stream momentum thickness is left unaltered as Γ is changed, it was found that the stability of mode II remains relatively unaffected. This suggests that θ_2 is a parameter of prime interest for the stability of the secondary stream.

To account for the strong dependence of the results on the choice of equation (2.6) to determine θ_2, we investigated the stability of profile 2 based on similarity solutions of the boundary layer equations (see Fig.2.2). The stability of this profile was found to be quite different from that of profile 1. Although mode I of profile 2 is essentially identical because the primary stream of this mode remains unaltered, mode II is considerably more unstable. Furthermore, the range of unstable wavenumbers α_r for mode II is much larger. This can be explained by the fact that the secondary stream of profile 2 is much sharper than for profile 1. Such sharp variations in r are generally associated with large wavenumbers α_r. This is exemplified by the fact that discontinuous profiles are unstable for all wavenumbers.

Our investigation of the new velocity profile indicates that the choice of profile is important factor in the overall stability, for any given θ_2. However, we also found that even when the profile is altered, the effect of θ_2 remains the same. According to the similarity solution used for profile 2, θ_2 decreases from 0.140 to 0.133 as the radius ratio Γ goes from 2 to 4. On the other hand, using equation (2.6) means that θ_2 increases from 0.140 to 0.220 for the same increase in Γ. As such, even though the instability decreased with Γ for profile 1 and increased with profile 2 (see Fig. 3.5 and Fig. 3.8), the important point is that in both cases the instability increased with decreasing momentum thickness θ_2. This serves to confirm that the momentum thickness θ_2 is a parameter of prime interest in the study of the stability of mode II.

Concluding Remarks

In this thesis, we have presented the results of an investigation of the stability of both plane and coaxial jets with velocity and temperature profiles characteristic of the exhaust region for a turbofan engine. The form of the profiles and the parameters that we varied were guided largely by experiments conducted by Papamoschou involving coaxial jets. We were particularly interested in how the stability of the jet would be influenced by the geometric effects, compressibility, the azimuthal wavenumber of the perturbation and the ratio of the velocities of the primary and secondary streams.

First, we conducted a comparison between a two-dimensional and an axisymmetric jet, the flow being incompressible. For the profiles under consideration, there are two modes of instability associated with either the primary or secondary streams. It was found that for profile 1 in the incompressible case, that the growth rate $-\alpha_i$ is very similar for the two-dimensional and axisymmetric cases for both modes. However, it was also observed that the two-dimensional and axisymmetric cases react differently to changes in geometry in that two-dimensional flows are more sensitive to such changes. We then described the effect of compressibility on the stability of the profile. We found that, overall, compressibility decreased the instability of the profile, except for low wavenumbers. As compressibility allows for the generation radiating modes travelling at ambient sound speed, it is noteworthy that some were observed here. These occurred in the hot profile for $M_0 \geq 0.8281$, though the critical value of M_0 can be decreased by increasing h.

Another conclusion derived from our analysis is that generally, the most unstable modes are those associated with the azimuthal number $m = 0$. However, if the profile is slowly varying in r, it is possible for the $m = 1$ modes to become more unstable than the $m = 0$ mode. The parameters determining which of the two profiles is more unstable were found to be θ_1/R_1 for mode I, mirroring Michalke's findings, while for mode II, the significant parameters were found to be both θ_2/R_1 and Γ.

The final element of analysis was the effect of velocity ratio h and radius ratio Γ on the stability of profile 1 and 2. It was observed that mode I was mainly influenced by h, while mode II was mainly influenced by the secondary stream momentum thickness θ_2, through the intermediary of Γ since $\theta_2 = \theta_2(\Gamma)$. The observed "independence" of the two modes, provided $\Gamma \geq 2$, has the benefit that it is straightforward to tune the instabilities. Specifically, it is simple to reduces instability of the most unstable mode, mode II, by increasing θ_2.

Future investigations on the stability of coaxial jets would most benefit from using non-parallel profiles. This would allow one to compute estimates of the radiated noise associated with the instabilities waves. Dahl and Morris [7] considered this problem for supersonic jets. To the best knowledge of the author, however, such an analysis hasn't been carried out for subsonic jets such as those studied in this thesis. Furthermore, the linear stability of slowly divergent axisymmetric jets in general could be supplemented by studying the propagation of wavepackets by solving the amplitude evolution equation derived in section 1.2. This theory could then be compared with Tam and Morris [23], or Dahl and Morris for coaxial jets, to determine if the predicted radiated noise is improved by a wave packet analysis.

Appendix A

Similarity Solution for the Velocity Profile 2

Profile 2 from Fig. 2.2 is derived by matching the primary stream of Profile 1 to the similarity solution of the boundary layer equations at a point r_m, which depends on the desired secondary radius R_2. The similarity solution then serves to describe the secondary stream and the outer region of the velocity profile. The advantage of this matched profile is that once the secondary radius R_2 is specified, the similarity solution determines the secondary stream momentum thickness, i.e. θ_2. Hence, by solving the boundary layer equations, we have designed a means to relate the secondary momentum thickness to the secondary radius, $\theta_2 = \theta_2(R_2)$.

As mentioned before, the boundary layer equations are the starting point for this solution. They are derived from the steady Navier-Stokes for incompressible flows

$$\boldsymbol{V} \cdot \boldsymbol{\nabla} \boldsymbol{V} = -\boldsymbol{\nabla} p + \nu \boldsymbol{\nabla}^2 \boldsymbol{V}, \tag{A.1}$$

and the continuity equation

$$\boldsymbol{\nabla} \cdot \boldsymbol{V} = 0\,. \tag{A.2}$$

To get the boundary layer equations for an axisymmetric flow from (A.1) and (A.2), a number of terms must be neglected. The neglected terms are those whose contributions are small in the boundary layers and they are determined using order of magnitude arguments (Ref. [4], p.27) based on the fact that variations accross the boudary layer are much larger than those parallel to the boundary layer. For axisymmetric flows, these simplifications take the form (Ref. [21], p.231)

$$u\frac{\partial u}{\partial x} + v\frac{\partial u}{\partial r} = \nu\frac{1}{r}\frac{\partial}{\partial r}\left(r\frac{\partial u}{\partial r}\right) , \tag{A.3}$$

and

$$\frac{\partial u}{\partial x} + \frac{\partial v}{\partial r} = 0 , \tag{A.4}$$

where the r-direction of (A.1) was neglected, while the θ-direction is zero for axisymmetric flows. One important assumption made in deriving (A.3) is that the pressure can be regarded as constant. This means that the flux of momentum in the x-direction is constant

$$J = 2\pi\rho\int_0^\infty u^2 r dr = \text{const} . \tag{A.5}$$

Just as in section 1.2, we can introduce a stream function defined as $\psi_r/r = u$ and $\psi_x/r = -v$ to solve (A.4). Substituting the stream function into (A.3), we get

$$\frac{1}{r}\left(\frac{\partial\psi}{\partial r}\frac{\partial^2\psi}{\partial x\partial r} + \frac{1}{r}\frac{\partial\psi}{\partial x}\frac{\partial\psi}{\partial r} - \frac{\partial\psi}{\partial x}\frac{\partial^2\psi}{\partial r^2}\right) = \nu\frac{\partial}{\partial x}\left(\frac{\partial^2\psi}{\partial r^2} - \frac{1}{r}\frac{\partial\psi}{\partial r}\right) . \tag{A.6}$$

We now look for a similarity solution to this equation by looking at a solution of the form (Ref. [21], p.231)

$$\psi \sim x^p F(\eta), \quad \text{where} \quad \eta = \frac{r}{x^n} . \tag{A.7}$$

By requiring that the solution satisfy equation (A.5) and that the friction and inertial terms in (A.3) be of the same order, we obtain that p and n are equal to 1. Substituting the similarity solution into equation (A.6), we obtain the equation

$$\frac{1}{\eta^2}\left(FF' - \eta F'^2 - \eta F F''\right) = \frac{d}{d\eta}\left(F'' - \frac{F'}{\eta}\right) . \tag{A.8}$$

Integrating by parts twice leads to the equation

$$F' = -\frac{F^2}{2\eta} + \frac{2F}{\eta} - \frac{C_1\eta}{2} + \frac{C_2}{\eta}\,. \tag{A.9}$$

In Schlichting's treatment of this equation (Ref. [21], p.232), the boundaries used, i.e. $\eta = 0$ and $\eta = \infty$, mean that C_1, $C_2 = 0$. However, taking the boundary condition at an arbitrary point $\eta_m = r_m/x \neq 0$ means that these constants do not necessarily vanish. A priori, the only requirement is that $\lim_{\eta\to\infty} \bar{u}(\eta) = 0$. This requirement means that $\lim_{\eta\to\infty} F'/\eta = 0$, and hence we conclude that

$$\lim_{\eta\to\infty} -\frac{F^2}{2\eta^2} + \frac{2F}{\eta^2} - \frac{C_1}{2} + \frac{C_2}{\eta^2} = 0\,. \tag{A.10}$$

So as $\eta \to \infty$, $F(\eta) \to 2 - \sqrt{4 - C_1\eta^2 + 2C_2}$, or equivalently

$$\bar{u} \to \frac{1}{2}\frac{C_1}{\sqrt{4 - C_1\eta^2 + 2C_2}} \propto \frac{1}{\eta}\,. \tag{A.11}$$

However, such a solution would imply that the momentum flux of the jet, $J \propto \int_0^\infty \bar{u}^2 r dr$, is infinite. To avoid this, it is necessary to take $C_1 = 0$.

It is now easy to solve (A.8). We first look for a particular solution, because (A.8) is a Ricatta's equation which has a solution of the form

$$F(\eta) = 1/f(\eta) + F_p(\eta)\,, \tag{A.12}$$

where F_p is a particular solution. Trying a to find a constant solution, $F_p =$ const., to (A.9), we get a quadratic equation for F_p

$$0 = -\frac{F_p^2}{2} + 2F_p + C_2\,. \tag{A.13}$$

Taking the root $F_p = 2 - \sqrt{4 + 2C_2}$ for convenience, we can now substitute (A.12) into (A.9) to find $f(\eta)$. The resulting equation is a non-homogeneous first order equation

$$f' + \gamma\frac{f}{\eta} = \frac{1}{2\eta}, \quad \text{where} \quad \gamma = \sqrt{4 + 2C_2}\,. \tag{A.14}$$

This equation is easily solved with the standard techniques, i.e. integrating factor and variation of parameter for first order equations.

Having solved equation (A.6) for the stream function, we can now compute the velocity profile for the secondary stream

$$u_s(\eta) = \frac{\nu\gamma^2 x}{2r^2}\left\{1 - \left[\tanh\left(\frac{1}{2}\ln\left(\frac{r}{x}\right)\gamma + \frac{\beta\gamma}{2}\right)\right]^2\right\}, \tag{A.15}$$

where β is a constant of integration. The constants β and γ are determined by matching u_s and u_s' with the primary stream u_1, from equation (2.1), at η_m, while x is chosen such that $\theta_2 = 0.14$ when $\Gamma = 2$, just as for profile 1. This matching of u_1 and u_s gives us the velocity profile 2 as shown in Fig. 2.2. It should be noted that the viscosity ν is unimportant since the resulting mean velocity profile $\bar{u}$ is normalized at $\eta = 0$.

Bibliography

[1] Batchelor, G. K., and Gill, A. E., Analysis of the stability of axisymmetric jets, *J. Fluid Mech.* **14**, 529-551 (1962).

[2] Benney, D. J., and Rosenblat, Stability of Spatially Varying and Time-Dependent Flows, *Phys. Fluids*, **7**, 1385-1386 (1964).

[3] Bouthier, M. Stabilité linéaire des écoulements presque parallèles, *J. de Mécanique* **11**, 599-619 (1972).

[4] Cebeci, T., *Modeling and Computation of Boundary-Layer Flows*, 2^{nd} edition, Springer-Horizons Publishing, (2005).

[5] Crighton, D. G., and Gaster, M., Stability of slowly diverging flow, *J. Fluid Mech.* **77**, 397-413 (1976).

[6] Crow, S.C., and Champagne, F.H., Orderly structure in jet turbulence, *J. Fluid Mech.* **48**, 547-591 (1971).

[7] Dahl, M. D., and Morris, P. J., Noise from supersonic coaxial jets, part 2: normal velocity profile, *J. Sound and Vibration* **200**(5), 655-699.

[8] Goldstein, M. E., A generalized acoustic analogy, *J. Fluid Mech.* **488**, 315-333 (2003).

[9] Howard, L. N.,The number of unstable modes in hydrodynamic stability problems, *J. de Mécanique* **8**, 433-443 (1964).

[10] Huerre, P., and Monkewitz, P. A., Absolute and convective instabilities in free shear layers, *J. Fluid Mech.* **159**, 151-168 (1985).

[11] Lighthill, M. J., On sound generated aerodynamically: I. General theory, *Proc. R. Soc. Lond.*, A **211**, 564-587 (1952).

[12] Lighthill, M. J., On sound generated aerodynamically: II. Turbulence as source of sound, *Proc. R. Soc. Lond.*, A **222**, 1-32 (1954).

[13] Lilley, G. M., On the Noise from Jets, *Noise Mechanism*, AGARD-CP-131, 13.1-12.12 (1974).

[14] Lin, C. C., *The theory of hydrodynamic stability*, Cambridge Univ. Press. (1955).

[15] Maslowe, S. A., editors: Swinney, H. L., and Gollub, J. P., *Hydrodynamic Instabilities and the Transition to Turbulence*, Springer-Verlag, 181-228 (1981).

[16] Michalke, A., Survey on jet instability theory, *Prog. Aerospace Sci.* **21**, 159-199 (1984).

[17] Michalke, A., On the influence of a wake on the inviscid instability of a circular jet with external flow, *Eur. J. Mech. B/Fluids*, **12**, 579-595, (1993).

[18] Morris, P. J., Jet noise prediction: past, present and future, *Canadian Acoustics* **35** (3), 16-22 (2007).

[19] Papamoschou, D., A new method for jet noise supression in turbofan engines," *AIAA Paper* 2003-1059, 1-13 (2003).

[20] Saric, W. S., and Nayfeh, A. H., Nonparallel stability of boundary layer flows, *Phys. Fluids*, **18**, 945-950 (1975).

[21] Schlichting, H., *Boundary-layer theory*, 7^{th} edition, Mc-Graw Hill, (1979).

[22] Talamelli, A., and Gavarini, I., Linear instability characteristics of incompressible coaxial jets, *Flow Turbulence Combust.* **76**, 221-240 (2006).

[23] Tam, C. K. W., and Morris, P. J., The radiation of sound by the instability waves of compressible plane turbulent shear layer, *J. Fluid Mech.* **98**, 349-381 (1980).

[24] Tam, C. K. W., and Burton, D. E., Sound generated by instability waves of supersonic flows. Part 1, two-dimensional mixing layers; Part 2, axisymmetric jets, *J. Fluid Mech.* **138**, 249-295 (1984).

[25] Tam, C. K. W., Jet noise: since 1952, *Theoret. Comp. Fluid Dyn.* **10**, 393-405 (1998).

[26] Tam, C. K. W. et al., The Sources of Jet Noise: Experimental Evidence, 13^{th} *AIAA/CEAS Aeroacoustics Conference* AIAA **2007-3641** (2007).